

**3D-Printed Ketoenamine Crosslinked Polyrotaxane
Hydrogels and Their Mechanochromic Responsiveness**

Journal:	<i>Polymer Chemistry</i>
Manuscript ID	PY-COM-03-2023-000337.R1
Article Type:	Communication
Date Submitted by the Author:	21-Apr-2023
Complete List of Authors:	Zheng, Dan; Dartmouth College, Chemistry Tang, Miao; Dartmouth College, Chemistry Ke, Chenfeng; Dartmouth College, Chemistry

COMMUNICATION

3D-Printed Ketoenamine Crosslinked Polyrotaxane Hydrogels and Their Mechanochromic Responsiveness

Dan Zheng,^{a†} Miao Tang,^{a†} and Chenfeng Ke^{*a}

Received 00th January 20xx,
Accepted 00th January 20xx

DOI: 10.1039/x0xx00000x

A ketoenamine-based dynamic covalent crosslinker was introduced to α -cyclodextrin-based polypseudorotaxanes, forming viscoelastic hydrogels for direct-ink-write 3D printing. The irreversible enol-keto tautomerization imparts high chemical stability to the extensively crosslinked polyrotaxane hydrogels, which showed mechanochromic responsiveness in the presence of the integrated fluorophores.

Dynamic covalent chemistry (DCC)^{1, 2} has been integrated into polymer designs as an enabler for self-healing³⁻⁵ and recycling properties.⁵ In these DCC networks, dynamic covalent bonding motifs, including imine,⁶⁻¹⁰ oximine,¹¹ boronic ester,^{12, 13} Diels-Alder adduct,¹⁴⁻¹⁷ disulfide,^{18, 19} and hydrazone,²⁰⁻²³ can form, dissociate, and exchange reversibly upon external stimuli.²⁴⁻²⁷ As such, DCC-based polymers have been developed as shape-morphing^{4, 16} and self-healing materials.^{11, 12, 17, 28} Among these DCC reactions, the reversible imine condensation has been used to construct direct-ink-write (DIW) 3D printing materials,^{22, 28} because the reversibility of imine bond formation and dissociation can facilitate the shear-thinning and self-healing properties required for DIW.^{29, 30} However, the chemical stability of imine linkages in these viscoelastic hydrogels are often concerning due to the abundant ambient water favoring the equilibrium towards the starting materials.^{7, 31} On the other hand, α -cyclodextrin (α -CD)-based polypseudorotaxanes have also been introduced as viscoelastic hydrogels for DIW,³²⁻³⁶ where the micro-crystalline domains formed between the polypseudorotaxanes serve to noncovalently crosslink the network.³⁶ The state-of-the-art polypseudorotaxane hydrogels utilize photo-crosslinking to afford 3D-printed polyrotaxanes, and they can exhibit a variety of stimuli-responsive properties

such as solvent-,³² pH-,³³ thermo-,³⁴ and moisture-responsiveness.³⁶ While photo-crosslinked hydrogels have been widely studied, hydrogels that can be crosslinked without needing photo-initiators and light irradiation will simplify the technical prerequisites for deployment, especially in biomedical environments.

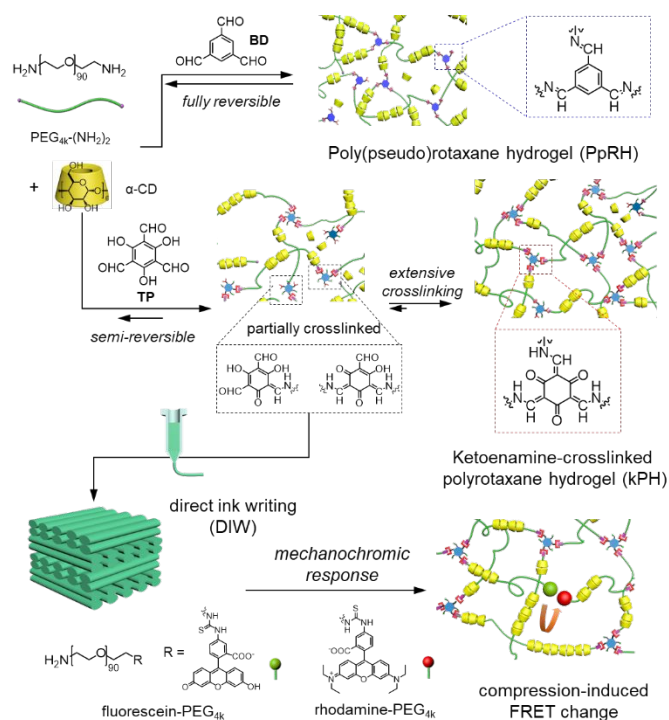


Fig. 1. Graphical illustration of the construction of 3D-printed polyrotaxane networks connected via dynamic covalent crosslinkages.

In this work, we integrate the dynamic imine network with the polypseudorotaxane hydrogel design, and expect the dual-crosslinked hydrogels to possess improved viscoelasticity for

^a Department of Chemistry, Dartmouth College, 41 College Street, Hanover NH 03755, United States

[†] These authors contributed equally to this work.

Electronic Supplementary Information (ESI) available: [details of any supplementary information available should be included here]. See DOI: 10.1039/x0xx00000x

DIW 3D printing while eliminating the need for photo-crosslinking, removing the concern of insufficient crosslinking due to limited light penetration.³²⁻³⁵ Herein, we introduce two dynamic crosslinkers, namely, 1,3,5-benzenetriolaldehyde (**BD**) and 1,3,5-triformylphloroglucinol (**TP**) to form DCC networks with α,ω -diamino-polyethylene glycol (PEG_{4k}-(NH₂)₂). The PEG_{4k}-(NH₂)₂ also serves as the axle for α -CD threading, forming a non-covalently crosslinked polypseudorotaxane network (Fig. 1). Different from the highly reversible imine-crosslinked network formed by **BD** and PEG_{4k}-(NH₂)₂, the reaction of **TP** with PEG_{4k}-(NH₂)₂ generates a more stable network due to the semi-reversible imine-to-ketoenamine tautomerization.³⁷⁻⁴⁰ In the presence of α -CDs, the polypseudorotaxane hydrogels crosslinked by these dynamic crosslinkers show different viscoelastic features. After extensive crosslinking, we discovered that the ketoenamine-based hydrogel showed good chemical stability against extensive washing, while the imine-crosslinked poly(pseudo)rotaxane hydrogel dissolved completely. After further appending rhodamine B and fluorescein moieties to the PEG axles, the generated ketoenamine-based polyrotaxane hydrogel showed mechanochromic response upon compression as a result of the Förster resonance energy transfer process.^{41, 42}

In our design, we chose a medium chain-length PEG_{4k} ($M_n = 4,000$ Da) as the axle because long-chain PEG-based hydrogels are difficult to be filtered out by human kidneys.⁴³ However, when an unfunctionalized PEG_{4k} axle is mixed with α -CD, white precipitates or brittle hydrogels are formed at different concentrations due to the crystallization of the α -CD-threaded polypseudorotaxanes.³⁶ Hence, we introduced DCC networks to improve the viscoelasticity of the polypseudorotaxanes.

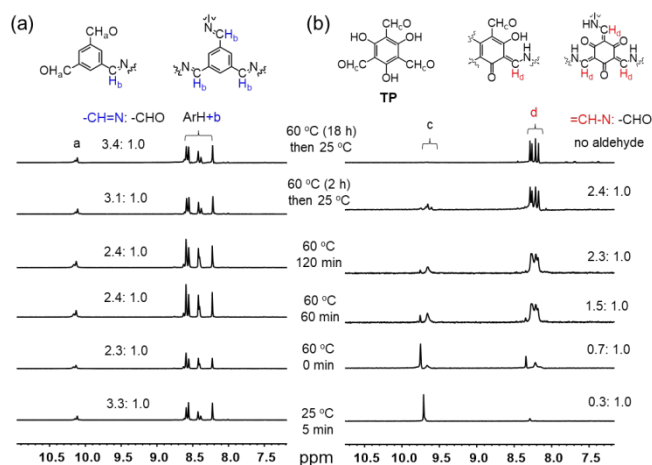


Fig. 2. (a) Temperature-varied time-dependent ¹H NMR spectra of PEG_{4k}-(NH₂)₂ (10.0 mM) and **BD** (6.7 mM) in D₂O at 298/333 K, revealing the highly dynamic feature of the imine bonds. (b) Temperature-varied time-dependent ¹H NMR spectra of PEG_{4k}-(NH₂)₂ (10.0 mM) and **TP** (6.7 mM) in D₂O at 298/333 K, suggesting the semi-reversible characteristic of ketoenamine bonds.

To understand the reversible features of the dynamic networks formed by PEG_{4k}-(NH₂)₂ and crosslinkers **BD** and **TP** in water, time-dependent ¹H NMR studies were performed at the same concentrations for the hydrogel formations in the absence of α -CD (Fig. 2). **TP** and PEG_{4k}-(NH₂)₂ were synthesized according to previously reported methods.^{33, 37} When **BD** and PEG_{4k}-(NH₂)₂ were mixed together, the reaction proceeded rapidly (5 min) at room temperature to form imine linkages (Fig. 2a). When the sample was heated to 60 °C, the imine formation was slightly reversed. The reaction equilibrium was re-established when the sample was cooled to room temperature, and the imine-to-aldehyde ratio resumed to that before heating. In contrast, **TP** was largely unreacted in the mixture of **TP** and PEG_{4k}-(NH₂)₂ at room temperature, and the reaction gradually proceeded at 60 °C (Fig. 2b). Two sets of aldehyde proton resonances were observed at 9.75 and 9.66 ppm, attributed to the unreacted and partially reacted **TP**, respectively. 2D NMR experiments (Fig. S5-6, S8-10) suggested that the proton resonances observed at 8.2 ppm are attributed to the ketoenamine moieties, and the population of imines is nearly negligible. After 18 h reaction at 60 °C, most **TP** had been converted to the ketoenamine linkages. These time-dependent ¹H NMR studies suggest that the rate of the reaction between **TP** and PEG_{4k}-(NH₂)₂ is much slower than that of **BD** and PEG_{4k}-(NH₂)₂, and the ketoenamine

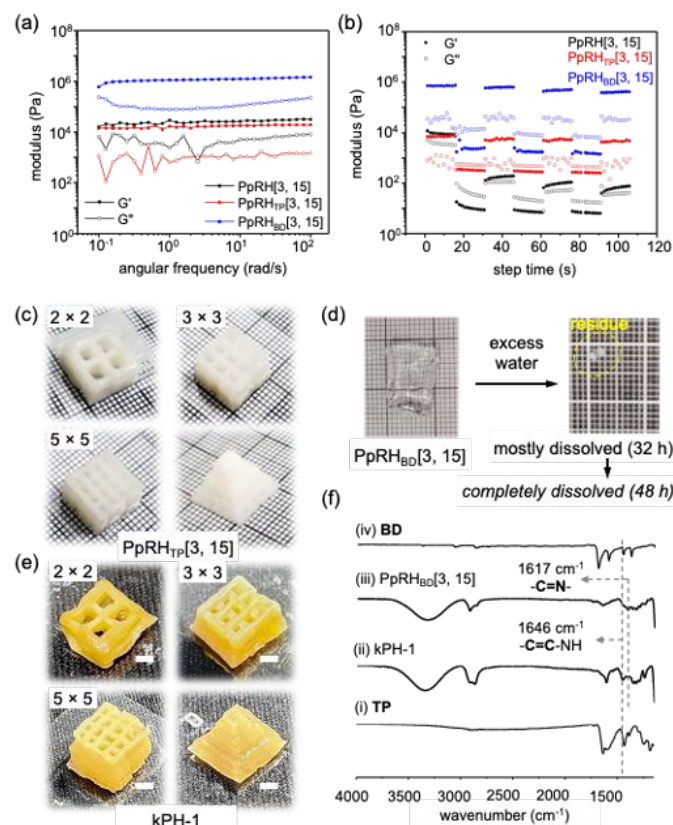


Fig. 3. (a) Angular frequency sweeps and (b) step-strain sweeps of PpRH[3, 15] (black), PpRH_{TP}[3, 15] (red), PpRH_{BD}[3, 15] (blue). (c) Images of 3D-printed cubic and pyramidal lattices printed with PpRH_{TP}[3, 15]. (d) Images of the degradation process of PpRH_{BD}[3, 15] in excess water. (e) Images of the kPH-1 monoliths

after extensive crosslinking. Scale bars: 2 mm. (f) FT-IR spectra of (i) **TP**, (ii) kPH-1, (iii) dehydrated PpRH_{BD}[3, 15], and (iv) **BD**.

In the presence of α -CD, the reactions of PEG_{4k}-(NH₂)₂ and dynamic crosslinkers **BD** and **TP** were heated at 60 °C for 2 h and then cooled down to room temperature, affording a series of viscoelastic hydrogels. Due to the dynamic covalent crosslinking, these hydrogels contain polyrotaxanes and polypseudorotaxanes, some of which are interconvertible. Hence, we name these samples poly(pseudo)rotaxane hydrogels (PpRHs[a, b]), in which a and b are the weight percentages of the PEG_{4k}-(NH₂)₂ and α -CD, respectively. At different ethylene glycol (EG) repeat unit to α -CD ratios (Table S1-2), PpRHs possess different viscoelastic properties in the rheological investigations (Fig. S15-45). When **BD** was used as the dynamic crosslinker, the elastic moduli of PpRH_{BD} hydrogels ranged between 10⁵-10⁶ Pa at a wide range of EG/ α -CD ratios (Fig. S33-45). For example, PpRH_{BD}[3, 15] possesses an elastic modulus $G' = 9 \times 10^5$ Pa in the angular frequency sweep (Fig. 3a), and excellent self-healing features in the step-strain studies (Fig. 3b). In comparison, PpRH[3, 15] formed by bare PEG_{4k} and α -CD has an elastic modulus of 2.5×10^4 Pa with a poor self-healing profile ($G' = 1.1 \times 10^2$ Pa after five cycles of step-strain sweeps, Fig. 3a-b). Furthermore, the PEG_{4k}-(NH₂)₂ and **TP** reaction mixture at the same concentration as the PpRH[3, 15] without α -CD did not yield any hydrogel. These results suggest that the microcrystalline domains of the poly(pseudo)rotaxanes remain the main contributor to the viscoelastic feature of the PpRHs, which is evident in the PXRD studies (Fig. S57).

When **TP** was used as the crosslinker, the elastic modulus of the PpRH_{TP}[3, 15] was recorded as 1.1×10^4 Pa in the angular frequency sweep (Fig. 3a), which is 100 times smaller than that of PpRH_{BD}[3, 15]. This result is consistent with the time-dependent ¹H NMR studies, in which the effective crosslinking density in the PpRH_{TP}[3, 15] is smaller than PpRH_{BD}[3, 15]. PpRH_{TP}[3, 15] also showed good self-healing properties in the step-strain studies as the elastic moduli fully recovered after five cycles of step-strain sweeps (Fig. 3b). When PEG_{4k}-(NH₂)₂, α -CD, and **TP** were heated for 18 h at 60 °C and then cooled down, the obtained hydrogel showed decreased elastic modulus ($G' = 1.3 \times 10^3$ Pa) and poorly self-healing properties (Fig. S16). In comparison, the PpRH_{BD}[3, 15] hydrogel did not show any reaction-time-dependent rheological variations (Fig. S33). These results revealed that both the imine and ketoenamine networks effectively promote the viscoelasticity features of PpRHs. However, as a result of the effective imine crosslinking, the viscosity of PpRH_{BD} hydrogels reached 10³-10⁴ Pa•s (Fig. S33), making them difficult to be extruded. In comparison, the viscosity of PpRH_{TP}[3, 15] hydrogels is 350 Pa•s (Fig. S16), which is suitable for DIW 3D printing. For example, 2 × 2, 4 × 4, and 5 × 5 piled grids and pyramids (40 layers) were 3D-printed using PpRH_{TP}[3, 15] (Fig. 3c).

The PpRH samples were heated to 70 °C overnight, cooled down, and immersed in excess water to examine their chemical stability. As a result of the high reversibility of the imine-crosslinked network, the PpRH_{BD}[3, 15] sample dissolved completely in water over 48 h (Fig. 3d). The soluble species were

also confirmed in the ¹H NMR experiment (Fig. S55). In contrast, the 3D-printed PpRH_{TP}[3, 15] samples were extensively crosslinked. The polypseudorotaxanes in PpRH_{TP}[3, 15] were converted to ketoenamine-based polyrotaxane hydrogels (kPH-1, Fig. 3e), and they are stable in excess of water (Fig. S56). IR spectra showed that the kPH-1 possesses a C=C stretching band at 1246 cm⁻¹ (Fig. 3f), compared to the C=N stretching band of the PpRH_{BD}[3,15] at 1644 cm⁻¹ (Fig. 3f). In a NaOD/D₂O solution (5 w/v%), the kPH-1 was hydrolyzed completely after being heated at 60 °C for 2 h. ¹H NMR spectrum (Fig. S47) showed that 10 α -CDs per PEG were mechanically interlocked in the kPH-1, corresponding to 22% of the PEG axes covered by α -CDs. Macroscopically, the 3D-printed kPH-1 showed good chemical stability and structural integrity in DMSO and water (Fig. 3e).

To study the mechanical performance of kPH-1, we performed tensile, cyclic (un)loading, and compression tests at room temperature (Fig. 4a-b). The Young's modulus and the compressive modulus of kPH-1 were measured as 214 kPa and 194 kPa, respectively (Fig. 4a). The strain at break of kPH-1 was measured as 260 % in the tensile test. kPH-1 was deformed to a strain of 93% in the compression test without breaking (Fig. 4a), showing good mechanical performance. In the cyclic (un)loading tests (Fig. 4b), the hysteresis of kPH-1 decreased gradually, suggesting the crystalline domains in the kPH-1 were disrupted during the elongation process but not fully reformed in each cycle.

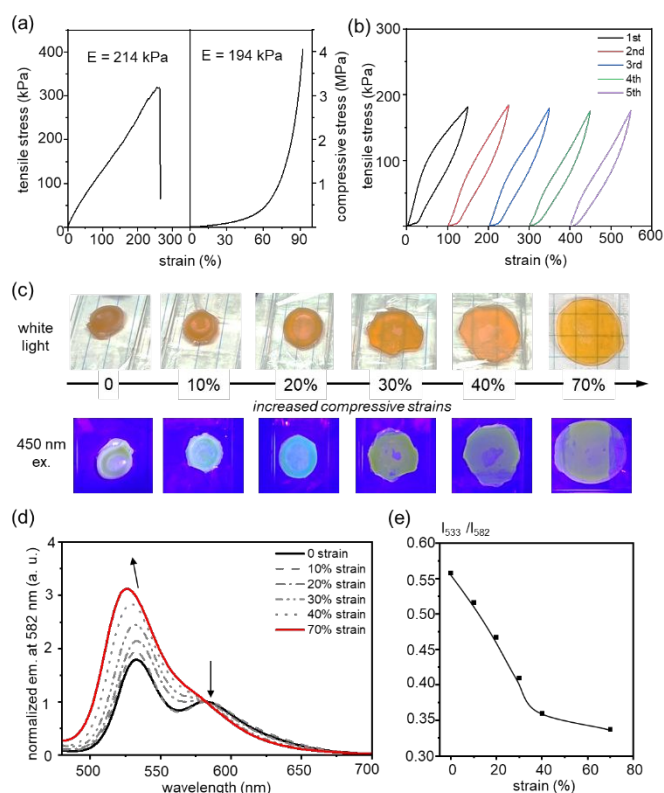


Fig. 4. (a) Uniaxial tensile and compression stress-strain profiles of kPH-1. Tensile strain rate: 1.5 mm/min, compression strain rate: 1 mm/min. (b) Multi-cyclic tensile (un)loading stress-strain profiles of kPH-1. Tensile strain rate: 1.5 mm/min. The profile is offset by 100% in each cycle. (c) Images of kPH-1 with doped PEG_{4k}-fluorescein and PEG_{4k}-rhodamine FRET pairs at different

compression strains under white light (top) and 450 nm light irradiation (bottom). (d) Fluorescence emission spectra of kPH-1 with doped FRET pairs at different compression strains. (e) The FRET efficiency (I_{582}/I_{533}) at different compression strains was calculated from (d).

To probe the structural change upon mechanical loading at the molecular level, we introduced a Förster resonance energy transfer (FRET) pair^{44, 45} to the kPH-1. Experimentally, a mixture of fluorescein and rhodamine-modified PEG axles (modification ratio = 1% for fluorescein/PEG and rhodamine/PEG) were used to construct the kPH_{FRET} (see the SI, Section 9). The orange-colored hydrogel was sandwiched between two glass slides, compressed to a determined strain, and subjected to fluorescent measurements. At 0% strain, the hydrogel emitted at 533 and 582 nm upon irradiation ($\lambda_{\text{ex}} = 450$ nm, Fig. 4d, black line). Upon compression, the emission at 582 nm decreased, and the emission at 533 nm increased (Fig. 4c and 4d). The decreased I_{582}/I_{533} values suggest that the averaged distances between two neighboring FRET pairs are increasing (Fig. 4e), corresponding to larger distances between PEG axles. Hence, the crystalline domains connecting the polyrotaxanes in kPH-1 were disrupted, which explained the decreased hysteresis upon cyclic loading.

Conclusions

In summary, we have successfully developed mechanically robust 3D-printed polyrotaxane hydrogels by integrating the dynamic covalent network with the noncovalently connected polypseudorotaxane network. We discovered that the highly reversible imine crosslinkages significantly improved the viscoelasticity of the polypseudorotaxane network, but the product gradually dissolved in excess water. In comparison, the ketoenamine crosslinkages improved the viscoelasticity of the poly(pseudo)rotaxane network for direct-ink-writing and provided good chemical stability after extensive crosslinking. Tensile and compression tests showed that the ketoenamine-crosslinked polyrotaxane hydrogels could be stretched to 260% and compressed to more than 93% with Young's modulus of 214 kPa. Furthermore, when Förster resonance energy transfer pairs were introduced to the polyrotaxane network, the hydrogel showed strain-dependent emissions, revealing the micro-environment changes upon compressing.

Conflicts of interest

There are no conflicts to declare.

Acknowledgments

This work is supported by the Department of Energy the Basic Energy Sciences DE-SC0022267. In addition, C.K. thanks the support of the Cottrell Scholar program from the Research Corporation for Science Advancement and the Beckman Young Investigator program from the Arnold and Mabel Beckman Foundation.

Notes and references

- S. J. Rowan, S. J. Cantrill, G. R. L. Cousins, J. K. M. Sanders and J. F. Stoddart, *Angew. Chem. Int. Ed.*, 2002, **41**, 898–952.
- Y. Jin, Q. Wang, P. Taynton and W. Zhang, *Acc. Chem. Res.*, 2014, **47**, 1575–1586.
- W. Zou, J. Dong, Y. Luo, Q. Zhao and T. Xie, *Adv. Mater.*, 2017, **29**, 1606100.
- Z. Li, R. Yu and B. Guo, *ACS Appl. Bio. Mater.*, 2021, **4**, 5926–5943.
- N. Zheng, Y. Xu, Q. Zhao and T. Xie, *Chem. Rev.*, 2021, **121**, 1716–1745.
- M. E. Belowich and J. F. Stoddart, *Chem. Soc. Rev.*, 2012, **41**, 2003–2024.
- A. Chao, I. Negulescu and D. Zhang, *Macromolecules*, 2016, **49**, 6277–6284.
- Y. Wang, K. Quevedo and E. Pentzer, *Polym. Chem.*, 2021, **12**, 2695–2700.
- K. P. Cortés-Guzmán, A. R. Parikh, M. L. Sparacin, A. K. Remy, L. Adegoke, C. Chitrakar, M. Ecker, W. E. Voit and R. A. Smaldone, *ACS Sustainable Chem. Eng.*, 2022, **10**, 13091–13099.
- Z. Zhang, D. Lei, C. Zhang, Z. Wang, Y. Jin, W. Zhang, X. Liu and J. Sun, *Adv. Mater.*, 2023, **35**, e2208619.
- M. Nadgorny, J. Collins, Z. Xiao, P. J. Scales and L. A. Connal, *Polym. Chem.*, 2018, **9**, 1684–1692.
- M. Nakahata, S. Mori, Y. Takashima, H. Yamaguchi and A. Harada, *Chem*, 2016, **1**, 766–775.
- L. L. Robinson, J. L. Self, A. D. Fusi, M. W. Bates, J. Read de Alaniz, C. J. Hawker, C. M. Bates and C. S. Sample, *ACS Macro Lett.*, 2021, **10**, 857–863.
- J. R. Davidson, G. A. Appuhamillage, C. M. Thompson, W. Voit and R. A. Smaldone, *ACS Appl. Mater. Interfaces*, 2016, **8**, 16961–16966.
- G. A. Appuhamillage, J. C. Reagan, S. Khorsandi, J. R. Davidson, W. Voit and R. A. Smaldone, *Polym. Chem.*, 2017, **8**, 2087–2092.
- G. Zhang, W. Peng, J. Wu, Q. Zhao and T. Xie, *Nat. Commun.*, 2018, **9**, 4002.
- A. Durand-Silva, K. P. Cortés-Guzmán, R. M. Johnson, S. D. Perera, S. D. Diwakara and R. A. Smaldone, *ACS Macro Lett.*, 2021, **10**, 486–491.
- Y. Liu, Y. Jia, Q. Wu and J. S. Moore, *J. Am. Chem. Soc.*, 2019, **141**, 17075–17080.
- Y. Deng, Q. Zhang, D. H. Qu, H. Tian and B. L. Feringa, *Angew. Chem. Int. Ed.*, 2022, **61**, e202209100.
- L. L. Wang, C. B. Highley, Y. C. Yeh, J. H. Galarraga, S. Uman and J. A. Burdick, *J. Biomed. Mater. Res. A*, 2018, **106**, 865–875.
- J. Lou, S. Friedowitz, K. Will, J. Qin and Y. Xia, *Adv. Mater.*, 2021, **33**, e2104460.
- E. Mueller, F. Xu and T. Hoare, *Biomacromolecules*, 2022, **23**, 4883–4895.
- V. G. Muir, T. H. Qazi, S. Weintraub, B. O. Torres Maldonado, P. E. Arratia and J. A. Burdick, *Small*, 2022, **18**, e2201115.
- P. Chakma and D. Konkolewicz, *Angew. Chem. Int. Ed.*, 2019, **58**, 9682–9695.
- J. M. Winne, L. Leibler and F. E. Du Prez, *Polym. Chem.*, 2019, **10**, 6091–6108.
- M. Podgórski, B. D. Fairbanks, B. E. Kirkpatrick, M. McBride, A. Martinez, A. Dobson, N. J. Bongiardina and C. N. Bowman, *Adv. Mater.*, 2020, **32**, e1906876.
- Y. Wang, P. Wei, Q. Zhou, C. Cipriani, M. Qi, S. Sukhishvili and E. Pentzer, *Chem. Mater.*, 2022, **34**, 5821–5831.

- 28 M. Nadgorny, Z. Xiao and L. A. Connal, *Mol. Syst. Des. Eng.*, 2017, **2**, 283–292.
- 29 L. Li, Q. Lin, M. Tang, A. J. E. Duncan and C. Ke, *Chem. Eur. J.*, 2019, **25**, 10768–10781.
- 30 M. Tang, Z. Zhong and C. Ke, *Chem. Soc. Rev.*, 2023, **52**, 1614–1649.
- 31 J. Hatai, C. Hirschräuser, J. Niemeyer and C. Schmuck, *ACS Appl. Mater. Interfaces*, 2020, **12**, 2107–2115.
- 32 Q. Lin, X. Hou and C. Ke, *Angew. Chem. Int. Ed.*, 2017, **56**, 4452–4457.
- 33 Q. Lin, L. Li, M. Tang, X. Hou and C. Ke, *J. Mater. Chem. C*, 2018, **6**, 11956–11960.
- 34 Q. Lin, M. Tang and C. Ke, *Polym. Chem.*, 2020, **11**, 304–308.
- 35 L. Li, Q. Lin, M. Tang, E. H. R. Tsai and C. Ke, *Angew. Chem. Int. Ed.*, 2021, **60**, 10186–10193.
- 36 Q. Lin, L. Li, M. Tang, S. Uenuma, J. Samanta, S. Li, X. Jiang, L. Zou, K. Ito and C. Ke, *Chem*, 2021, **7**, 2442–2459.
- 37 J. H. Chong, M. Sauer, B. O. Patrick and M. J. MacLachlan, *Org. Lett.*, 2003, **5**, 3823–3826.
- 38 M. Sauer, C. Yeung, J. H. Chong, B. O. Patrick and M. J. MacLachlan, *J. Org. Chem.*, 2006, **71**, 775–788.
- 39 P. Kieryk, J. Janczak, J. Panek, M. Miklitz and J. Lisowski, *Org. Lett.*, 2016, **18**, 12–15.
- 40 S. Bera, A. Basu, S. Tothadi, B. Garai, S. Banerjee, K. Vanka and R. Banerjee, *Angew. Chem. Int. Ed.*, 2017, **56**, 2123–2126.
- 41 J. W. Neubauer, N. Hauck, M. J. Männel, M. Seuss, A. Fery and J. Thiele, *ACS Appl. Mater. Interfaces*, 2019, **11**, 26307–26313.
- 42 T. M. Khang, R. Huang, A. Khan, W.T. Chuang, P. Q. Nhien, T. T. K. Cuc, B. T. B. Hue, K.H. Wei, Y.K. Li and H.C. Lin, *ACS Materials Lett.*, 2022, **4**, 2537–2546.
- 43 B. Jeong, Y. H. Bae, D. S. Lee and S. Kim, *Nature*, 1997, **388**, 860–862.
- 44 K. E. Sapsford, L. Berti and I. L. Medintz, *Angew. Chem. Int. Ed.*, 2006, **45**, 4562–4589.
- 45 P. Rajdev and S. Ghosh, *J. Phys. Chem. B*, 2019, **123**, 327–342.